ISSN 1392–1207. MECHANIKA. 2018 Volume 24(4): 404–411

Finite Element Analysis of Dynamic Fracture Behaviour of Drill Pipe under Various Impact Loads

Guanghui ZHAO*, Li ZHAO, Y.X. ZHANG***, Ju LI******
**School of Mechanical Engineering, Southwest Petroleum University. Key Laboratory of Oil and Gas Reservoir Geology and Exploitation (Southwest Petroleum University), Chengdu, China, E-mail: zhaogh@swpu.edu.cn*
***AECC Chengdu Engine Co., Ltd. Chengdu, China, E-mail: 993945753@qq.com*
****School of Engineering and Information Technology, The University of New South Wales, Canberra, Australia, E-mail: Y.Zhang@adfa.edu.au*
*****CMEE, Sichuan Agricultural University, Ya'an, China, E-mail: 1175495369@qq.com*

crossref http://dx.doi.org/10.5755/j01.mech.24.4.19503

1. Introduction

Drill pipes (DPs) are the main tools for drilling oil and natural gas wells. According to statistics, the regions of the DP near the well head and near the bottom hole assemblies (BHA) are more prone to fracture failures. The DP near the well head is subjected to significant tension during drilling and tripping, which causes tremendous tensile impacts in cases of sudden raising and braking. In addition, rotary drilling systems often experience complicated loading in working conditions, such as severe stick-slip vibration, bit bouncing and self-excited vibration with parameters varying in unstable range [1]. All these complicated impact loads can be broken down into elementary impacts such as tensile, eccentric compressive, torsional impact loading and transverse collision with well wall.

A few researches on DP failure were reported, for example, fatigue failures of DPs caused by vibration [2], erosion wear generated by drilling fluid containing debris [3], static fracture characteristics studied by a cohesive zone model [4]. The effects of impact loading on dynamics responses of DPs with cracks and their fracture failure were rarely studied. In fact, the impact loads which are applied repeatedly to the DP act just like a cyclic load. Fig. 1, a and Fig. 1, b [5] shows the fatigue fracture and twist-off fracture of the DPs from rig site. Thus it is necessary to take the dynamic effects into consideration for accurate and reliable prediction of the service life of a DP.

a b

Fig. 1 Broken DPs from rig site: a – fatigue fracture; b – twist-off fracture [5]

From the fracture appearances of the DPs on a well site, it was found that most of fracture failures were induced by dynamic propagation of cracks, which were initiated from a small defect. Lin & Smith [6] and Carpinteri [7] found that any initial circumferential surface defects with an arbitrary shape in cylindrical bars would develop asymptotically into a semi-elliptical shape with a certain aspect ratio after a few fatigue cycles. Therefore, a semi-elliptical surface crack was often used to represent the defect in a DP, and the problems with a circumferential crack lying at the outer surface of a hollow cylinder were mainly studied by means of numerical methods due to complexity of the problems [8].

Regarding dynamic fracture behaviours, the published literatures mostly focused on two-dimensional cracks [9, 10]. The papers published on three-dimensional (3-D) cracking mainly focused on infinite or semi-infinite cracked body [11, 12]. Only few works have been devoted to the 3-D crack of an object of a finite dimension. For example, Guo et al. [13] developed a 3-D FE program and investigated thermal-elastic dynamic fracture of a hollow cylinder with a semi-elliptic surface crack under thermal stress and impact inner pressure. The effects of the hollow cylinder's boundary surface, crack surface, material inertia and stress wave interactions on the dynamic fracture behaviours of the cylinder were reported.

In this study, a finite element (FE) model is developed and used to capture 3-D dynamic fracture responses of a defected DP under various elementary impact loads, including tension, eccentric compression, torsion and transverse collision between the DP and borehole wall. The defect is simplified as a 3-D circumferential semi-elliptical surface crack on the outer surface of the DP, and inertial effects on the crack driving force are evaluated.

The paper is structured with 5 main sections. To begin with, mechanical models corresponding to longitudinal and transverse loading scenarios of DPs are established in Section 2. Then an FE model to simulate the dynamic fracture of the DP is developed and validated in Section 3. Dynamic responses of the cracked DP under various impact loads are presented in Section 4. Finally, concluding remarks are given.

2. Mechanical models of drill pipes subjected to impact loads

For drill pipes which are widely used to drill oil and natural gas wells, four kinds of elementary impacts, i.e. tension, eccentric compression, torsion and transverse collision with borehole wall, compose almost all the complex impact loads. Tensile impact happens to the DP near the well head in cases of sudden raising and braking, and the other three kinds of elementary impacts usually happen to the DP near the BHA. Eccentric compression and torsion are

due to DP whirling, bit bouncing and sticking, and serious transverse collision usually happens due to parametric resonance in rotary drilling systems. In this section, the mechanical models of DPs under the longitudinal loading scenario including tensile, eccentric compressive and torsion impacts, and under the transverse loading scenario are established.

The DP discussed in this study is made of G105 steel with Young's modulus E of 206 GPa and Poisson's ratio v of 0.289, and it is used in drilling ultra-deep wells with a borehole diameter of D = 314 mm. The outer diameter of the DP is d = 127 mm and its thickness is t = 9.19 mm (Fig. 2). A crack is simplified as a semi-elliptical crack located on the external surface of the DP. The major axis and minor axis of the crack are denoted as a and c, respectively, and the characteristic dimension of the crack is described by the dimensionless parameters a/t and a/c, the so-called crack depth ratio and aspect ratio.

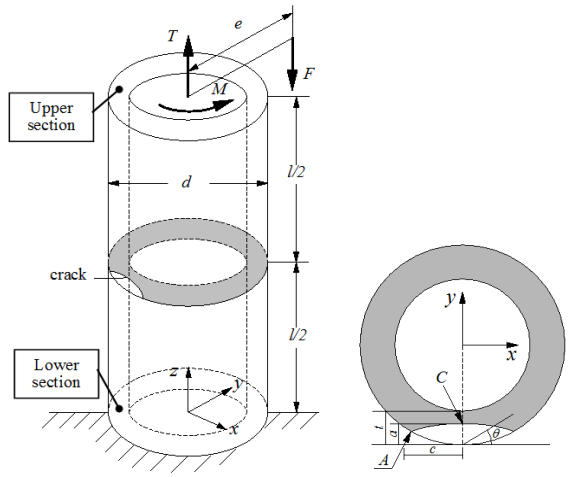

a b

Fig. 2 Mechanical model of the cracked DP under longitudinal impact loads: a – the cracked DP; b – the cracked cross-section

2.1. Longitudinal loading scenario

A segment of DP of a total length l = 2 × 500 mm is employed for the dynamic analysis subjected to longitudinal impact loading and the geometry and loading are shown in Fig. 2, a. The crack is assumed to locate in the middle section of the DP segment, and the symmetric axis of the crack is along the y direction (Fig. 2, b). Here a/t is chosen as 0.2, and the aspect ratio a/c as 0.8 which is close to the transition aspect ratio under this crack depth [14]. An arbitrary point on the crack front is determined by θ.

To model the longitudinal impact loading, the lower section of the DP is constrained, while the upper section is free and loaded by impact surface loads of tension T, eccentric compression F and torsion M, respectively. The tensile impact load is expressed as:

$$T(t) = \begin{cases} T_0 \cdot t / t_0, & 0 \le t \le t_0 \\ T_0, & t > t_0, \end{cases} \tag{1}$$

where: T_0 is the amplitude of the load, and t_0 is ramp loading time, which characterises the loading rate. The eccentric compressive and torsion impact loads are of the same form described in Eq. (1) given that T is replaced by F and M, respectively. The action lines of tension and torsion coincide with the central axis of the DP, while the action line of compressive force F shifts an eccentricity e, derived as $e = (D - d) / 2$, from z-axis in the y direction for the eccentric compressive impact as illustrated in Fig. 2, a. It corresponds to the condition that the cracked cross-section of the DP touches the borehole wall when compressive impact waves due to bit bouncing arrives. Here, the basic loading parameters are chosen as T_0 = 1050 kN, F_0 = 360 kN, M_0 = 10 kN·m and the time of the ramp loading is set as t_0 = 10 μs.

2.2. Transverse loading scenario

Since the outer diameter of the tool joint of the DP is larger than its body (Fig. 3, a), collisions between DP and borehole wall always happen at the tool joint. The collision time is normally a few to ten milliseconds and impact forces could reach hundreds of kilo-newtons according to the characteristics of sidewall rock [15, 16]. To simplify the analysis, the following assumptions are made: 1. only the joint of DP contacts the borehole wall, and all the joints of the DP collide with the borehole wall simultaneously; 2. the head-on collision happens between joints and wall; 3. the effect of drilling fluid is ignored during collision; 4. the rotation of the DP is not taken into account.

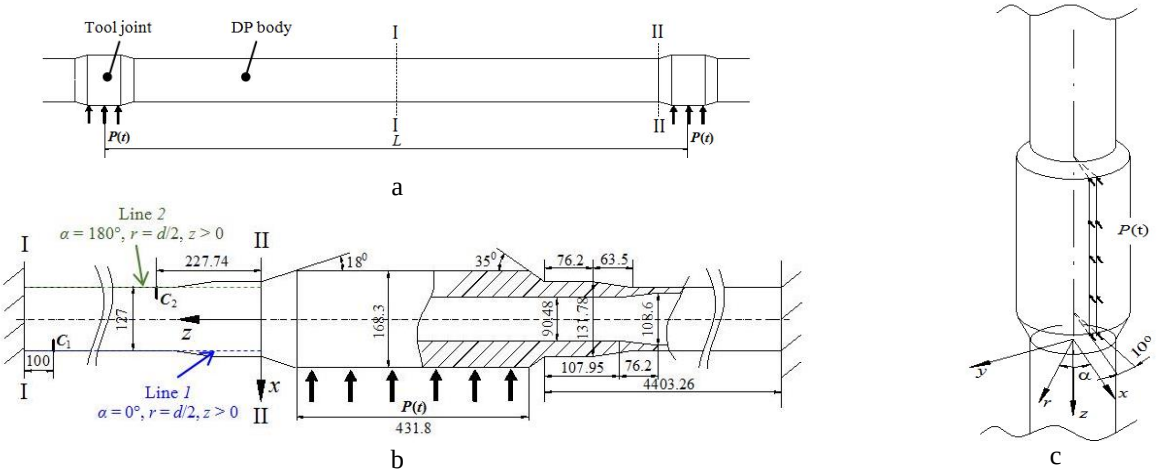

Fig. 3 Mechanical model of the DP under transverse collision with sidewall: a – sketch of the DP; b – mechanical model; c – tool joint with loading area (Length unit, mm)

Based on the second assumption and the fact that geometry and loading condition of the DP are all approximately symmetric about the middle section *I-I* of the DP (Fig. 3, a), section *I-I* cannot rotate or move axially and is set as fixed here. The mechanical model of the DP is then established by the two adjacent half DPs as presented in Fig. 3, b, which also shows the structure of the studied DP which is an internal-external upset DP with a total length of L = 9,600 mm. The transverse impact force $P(t)$ is represented as a half sinusoidal wave with amplitude of P_0 = = 150 kN lasting for 5 ms, which is applied on a narrow area of the external surface of joint (10 degrees in central angle) as shown in Fig. 3, c.

3. Finite element analysis of drill pipe

Based on FE theory of 3-D crack problems, an FE model is developed for dynamic analysis of a DP with a circumferential semi-elliptical crack on the outer surface under various impacts. A convergence study is conducted to determine the time step and space step for the dynamic FE analyses. Then the FE model was validated to ensure the correctness of the subsequent analysis.

3.1. Dynamic finite element analysis of 3-D crack problem

For a 3-D crack under impact loading, dynamic *J*-integral method, which is independent of the domain used and robust even with coarse meshes, is used to calculate the dynamic stress intensity factor (SIF) along the crack front in this study.

Based on the elastodynamic responses of stress σ_{ij} (i, j = 1, 2, 3) and displacement u_i (i=1, 2, 3), which are obtained using the technique of explicit time integration in FE analysis of the cracked body, the dynamic *J*-integral (denoted as J^d) is calculated as a post-processor by a volume integral, which is derived from a contour integral applying the divergence theorem, and the virtual crack extension method. It is written as:

$$J^d = \int_V \left[\left(\sigma_{ij} u_{i,k} - U\delta_{kj} \right) q_{k,j} + \rho \ddot{u}_i u_{i,k} q_k \right] dV, \qquad (2)$$

where: V is a domain whose boundary surface is a small tubular surface S enclosing the crack line. U is the elastic strain energy and δ_{kj} (k, j = 1, 2, 3) is the unit tensor. ρ is mass density of the material and a superposed dot denotes the time derivative. $q_k = ql_k(s)$ is weighting vector, in which q is a weighting function varying from one on the crack front to zero on boundary surface S, and the l_k(s) is a dimensionless vector whose norm varies from zero to one to describe the shape of the extended crack front at the position s of the crack line. The parameter s is the curvilinear coordinate along the crack front and denotes the crack front. For more details of the dynamic *J*-integral method one may refer to the work by Enderlein, et al. [17] and Shih, et al [18].

Then the dynamic SIFs, K_I^d, K_{II}^d and K_{III}^d, are derived from the dynamic *J*-integral. The SIFs, which are usually used to characterize the local crack-line stress and displacement fields, are related to the *J*-integral as shown in Eq. (3).

$$J^d = \frac{1}{\bar{E}} \left[\left(K_I^d \right)^2 + \left(K_{II}^d \right)^2 \right] + \frac{1}{2G} \left(K_{III}^d \right)^2, \qquad (3)$$

where: $\bar{E} = E/(1-\nu^2)$ for plane strain problems and $\bar{E} = E$ for plane stress problems. E and ν are Young's modulus and Poisson ratio, respectively, and G is shear modulus. Note the SIFs and *J*-integral are time-dependent. For the mode I and mode III cracks, SIFs could be derived from *J*-integral and expressed by Eq. (4):

$$K_I^d = \sqrt{\bar{E} \bullet J^d}, \qquad K_{III}^d = \sqrt{2G \bullet J^d}. \qquad (4)$$

In the following sections, the dynamic SIFs of the cracked DP are calculated by FE method, and dynamic effects of various elementary impact loads on the crack driving force are evaluated.

3.2. The finite element model

FE analysis is conducted using Abaqus to simulate the elastodynamic responses of the cracked DP, and the results of stress and displacement are extracted to calculate the fracture parameters. In this section, FE models under various longitudinal impacts, including tension, eccentric compression and torsion, are presented and discussed. After validation, the FE model would be generalized to the scenario of the pipe under transverse impact.

The structured-meshing technology is employed to discretize the whole DP model. In order to generate regular hexahedral grids, the cracked cross-section is first divided into several zones (Fig. 4), in which the curve *ABC* is a half crack front with the deepest point denoted as *C* and the edge point as *A*. The curve *DEF* and *GHI* are both elliptical lines. 10 nodes are set evenly for the crack front *AB* and *BC*, respectively. The zoning line *CF* and *CI* that are normal to the crack front are divided into 10 uneven parts respectively according to the geometric progression, which takes the crack tip *C* as a starting point. In the direction of *z*-axis, the upper half ($l/2 \le z \le l$) is divided into two parts. The first interval is $l/2 \le z \le 5l/8$ and the second is $z > 5l/8$.

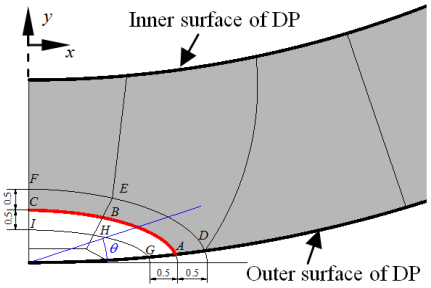

Fig. 4 Partition sketch of partial cracked cross-section (Length unit: mm)

Fig. 5 illustrates the FE mesh of a quarter of the DP and the refined mesh around the crack front as an example. Starting from the cross section $z = l/2$ (namely, the location of the crack surface), 40 nodes are set nonhomogeneously in the first interval, which is $l/8$ long, according to geometric progression. For the second interval ($z > 5l/8$), the mesh size in the *z*-direction remains the same as that of $z = 5l/8$. In the FE model, the eight-node linear brick element with reduced integration denoted as C3D8R is employed, and there are 268,750 of nodes and 247,360 of elements totally employed in the FE model.

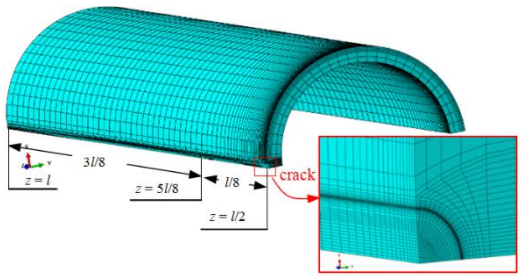

Fig. 5 FE mesh of a quarter of the DP model and mesh refinement around the crack front

At each time step, 10 contour integrals are extracted around the point of the crack front in the plane perpendicular to the crack line, in which the average value of contour integrals from the 4th to the 8th is defined as dynamic *J*-integral for this point. Then dynamic SIFs are deduced from the dynamic *J*-integral. For convenience, dynamic SIF, K_i^d (i = *I, II, III*), under longitudinal impact loads of tension, eccentric compression and torsion, described in Eq. (1), is normalized with respect to the static SIF, K_i^s (i = *I, II, III*). The static SIFs are obtained under static tensile load T_0, static eccentric compressive load F_0 and static torque M_0, respectively, at the same point as that of K_i^d, and they are expressed as:

$$K_{0i}^d = K_i^d / K_i^s, \quad i = I, II, III, \tag{5}$$

where: K_{0i}^d (i = I, II, III) is the dimensionless dynamic SIF for longitudinal impact loads.

3.3. Convergence study

Convergence study is conducted to determine the appropriate space step and time step for modelling the dynamic responses of the cracked DP herein.

A convergence study related to space step is conducted under static tensile loading. For the static tensile loading, the dimensionless SIF, K_{0I}^s, is defined as:

$$K_{0I}^s = K_I^s / \left(\sigma\sqrt{\pi a}\right), \tag{6}$$

where; σ is the nominal tensile stress at the crack.

To obtain different element dimensions for the FE mesh of the DP, a refinement factor n is introduced and described as follows. Referring to Figs. 4 and 5, the crack fronts *AB* and *BC* are refined n times by setting 10n nodes respectively and homogeneously, and *CF* and *CI* are set 10n nodes respectively according to the geometric progression. 40n nodes are inserted unevenly along the z-axis within $l/2 \le z \le 5l/8$ of the crack on the basis of geometric progression. With different mesh densities, K_{0I}^s on the crack front as a function of θ is computed and shown in Fig. 6. It's found that K_{0I}^s at the deepest point *C* of crack front (θ = 90°) is not sensitive to mesh density, while K_{0I}^s varies greatly near the outer surface point *A* of the DP ($\theta \approx 0°$). Taking the result corresponding to the mesh case of n = 1.4 as reference, the maximum relative errors of K_{0I}^s, which happens at point *A*, are calculated and listed in Table 1. It is concluded that the numerical results are converged with mesh refining. The results from the mesh with n = 1 are almost consistent with those from the mesh with n = 1.4, and the relative error of K_{0I}^s is only 0.7% for point *A* between these two cases. Considering both computation effectiveness and accuracy, the FE mesh with n = 1 as shown in Fig. 5 is used to simulate the fracture behaviour of DP, and is further extended to modelling the dynamic responses of the cracked DP under various impact loading.

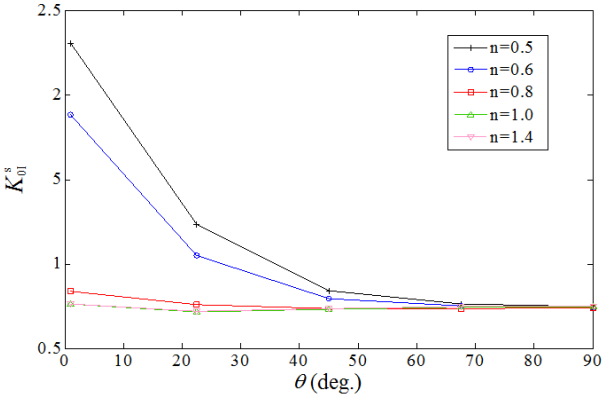

Fig. 6 K_{0I}^s along the crack front with different mesh densities (n = 1 corresponding with the mesh model of Fig. 5)

Table 1

Relative errors of K_{0I}^s at Point *A* corresponding to different mesh densities

Refinement factor n	1.4	1	0.8	0.6	0.5
Relative error (%)	0	0.7	9.6	145.5	201.0

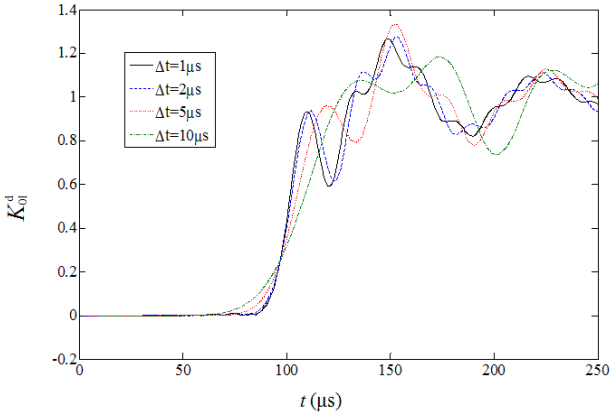

Fig. 7 Effect of different time steps on K_{0I}^d

Convergence study about time step is conducted under tensile impact T that is formulized in Eq. (1). In order to avoid influence of waves reflected from both ends on the crack, the dynamic response of the cracked DP is simulated for 250 μs. Time step Δt is chosen as 1 μs, 2 μs, 5 μs and 10 μs, respectively. The predicted time history of K_{0I}^d at the deepest point *C* of the crack with Δt is shown in Fig. 7. When Δt decreases, the numerical solution becomes stablized and converged, and the results obtained with Δt = 2 μs agree well with those with Δt = 1 μs, with only a 0.5% error for the peaks. Thus the time step of 2 μs is adopted in following simulations. Meanwhile, the time

histories of the contour integrals from the 4th to the 8th at point *C* are compared, and it is found that the maximal relative error is only 0.4%, meaning that conservation of dynamic *J*-integral is also ensured.

3.4. Numerical verification

Due to the lack of experimental results of dynamic fracture behaviour of a hollow cylinder with a circumferential semi-elliptical crack on the outer surface under impact loading, the present numerical model is verified in terms of the fracture behaviour under static loading, including tension, torsion and bending. The predicted results are compared to those reported in other literatures. For the mode I loading condition, the dimensionless SIF K_{0I}^{s}, which applies to both tension and bending, is given by Eq. (6). Similarly, the dimensionless SIF, K_{0III}^{s}, for mode III loading applying to torsion is defined as:

$$K_{0III}^{s} = K_{III}^{s} \Big/ \left(\tau\sqrt{\pi a}\right), \tag{7}$$

where: τ is the nominal shear stress at the crack.

Under the static loading condition of tension, torsion and bending, the computed K_0^s at both the deepest point *C* and the edge point *A* of the crack front, derived from *J*-integrals, are compared with those obtained by Newman, et al. [19] Wang, et al. [20] and Chen, et al. [21], respectively, which are all adopted in Handbook of the stress intensity factor [22], as presented in Table 2. It is found that the maximum relative error of the K_0^s is only 4.2%. In addition, the relative error between the average *J*-integral and corresponding 5 contour integrals (from the 4th to the 8th contour) is computed. The maximum value is only 0.7%, which means that path independence of the static *J*-integral is assured very well. This demonstrates that the present FE model could simulate the response of the cracked DP under static loading well.

Table 2

The computed K_0^s of the cracked DP under static tension, torsion and bending loads

Load	K_0^s	Point *A*	ε (%)	Point *C*	ε (%)
Tension	K_{0I}^s (present model)	0.728	1.9	0.745	0.1
	K_{0I}^s [19]	0.742		0.746	
Torsion	K_{0III}^s (present model)	0.642	1.1	0.649	3.5
	K_{0III}^s [20]	0.635		0.627	
Bending	K_{0I}^s (present model)	0.771	3.9	0.714	4.2
	K_{0I}^s [21]	0.742		0.745	

For the effectiveness of the present FE model in simulating dynamic fracture responses of the cracked DPs, confidence is gained from the convergence corresponding to time step and path independence of the predicted dynamic *J*-integral, which are presented in Section 3.3. Therefore, the present FE model and mesh is expected to be able to simulate dynamic crack under various impact loading. It should be noted that in the following calculations the *J*-integral values are extracted only at the deepest point *C* ($\theta = 90^o$).

4. Dynamic response of DP under various impact loads

Employing the developed FE model, dynamic responses of the cracked DP are investigated under each elementary impact load, and the inertial effects of the impact loading on the dynamic SIFs are evaluated.

4.1. Dynamic response of DP under longitudinal impact

Longitudinal impacts including tensile, eccentric compressive and torsional impacts, are discussed in this section.

4.1.1. Tensile impact

Loaded by the tensile impact with different loading rate, which is characterized by a ramp loading time, t_0, the dynamic responses of the cracked DP are computed and evaluated. The K_{0I}^d with varying t_0 of 5, 10, 20 and 50 μs is shown in Fig. 8. Due to reflection and interference of the stress waves from the inner and outer surfaces of the DP and the crack surface, several peaks appear. The greater the loading rate, i.e. the less t_0 is, the larger the K_{0I}^d peak is. For $t_0 = 5$ μs, the peak of dynamic SIF is 1.314 times of the value at the static loading condition.

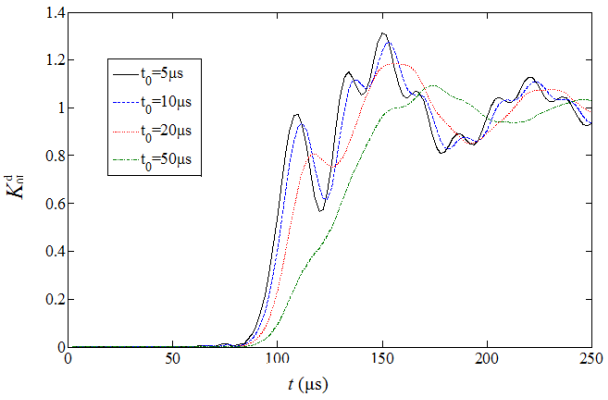

Fig. 8 Effect of loading rates on K_{0I}^d under tensile impact

4.1.2. Eccentric compressive impact

For the cracked DP, the up-going stress waves corresponding to eccentric compressive impact are made up of longitudinal compressive waves and bending waves. Here the analyzing time is set as $t = 250$ μs to avoid the influence of the upper and lower boundary surfaces of the DP model on the dynamic response of the crack.

Fig. 9 presents the time histories of K_{0I}^d under eccentric compressive impact with different loading rates. Bending wave is a dispersive wave and the wave velocity is different from that of the longitudinal wave. Waves reflecting from the crack surface interferes with that from the inner and outer surfaces of the DP. Therefore, the dynamic responses of K_{0I}^d show characteristics of complexity. K_{0I}^d diminishes somewhat with a decrease in loading rate and the maximum value of K_{0I}^d is only 1.025. In most cases, K_{0I}^d is below 1, which means that the crack driving force is weaker under dynamic loading of eccentric compression compared to that under corresponding static load.

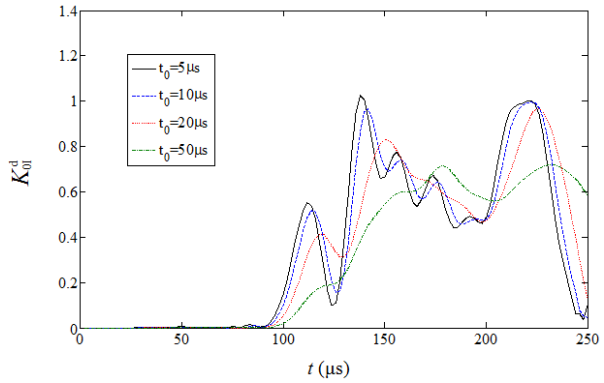

Fig. 9 Effect of loading rates on K_{0I}^d under eccentric compressive impact

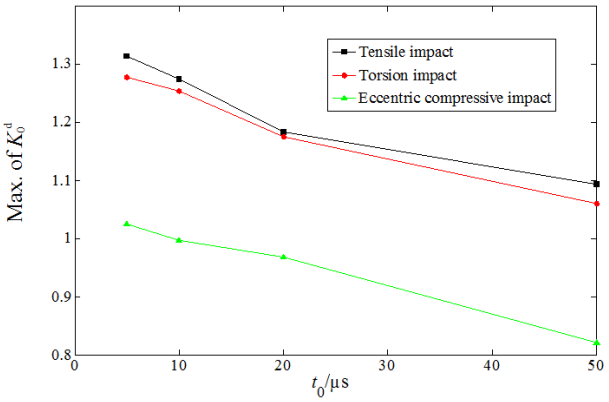

Fig. 11 The maximum value of K_0^d versus loading rate for different longitudinal impacts

4.1.3. Torsion impact

To avoid influences of reflected waves from both ends of the DP model, the torsion impact is assumed to last for 450 μs. Under the torsional impacts with different loading rates, changes of K_{0III}^d over time are computed as shown in Fig. 10. Being different from the complicated dynamic responses under tensile impact or eccentric compressive impact, the time histories of K_{0III}^d under torsion impact are all regular decadent waves with a period of 30 μs or so and approach 1 at last, namely, the static state. The maximum value of the K_{0III}^d increases with the increase of the loading rate. Under the ramp loading time of t_0 = 5 μs the peak value of K_{0III}^d is 1.277 times of the corresponding static value. In the case of t_0 = 50 μs the greatest value of K_{0III}^d is only 1.060 and the dynamic effect almost vanishes.

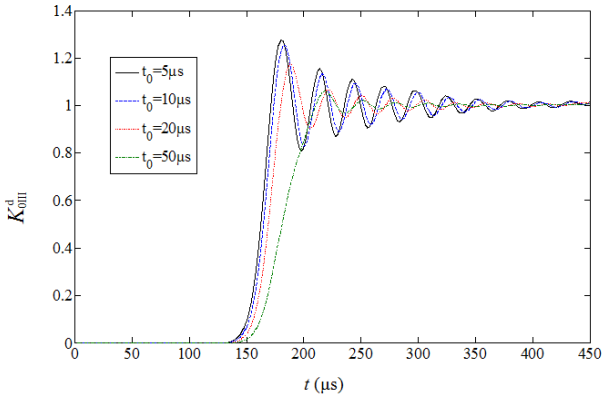

Fig. 10 Effect of loading rates on K_{0III}^d under torsion impact

Under these three kinds of longitudinal impacts, the peak values of dynamic SIFs generally rise with the increase of the loading rate as shown in Fig. 11. It is found that the tensile impact presents dynamic effect most prominently, followed by the torsion impact. The eccentric compressive impact contributes the least to the dynamic fracture of the DP. Under the actual loading condition with frequent tensile and torsional impacts, the dynamic effect of the impact loading on fatigue life prediction of the DP must be taken into consideration.

4.2. Dynamic response of DP under transverse collision

The dynamic response of an internal-external upset DP as shown in Fig. 3, b is modelled using the developed FE model. The dangerous position of the DP is identified firstly under collision according to stress analysis of a perfect DP, and then the DP with a crack at the dangerous location is simulated. The influence of stress wave caused by the collision on the dynamic crack driving force is evaluated.

Firstly, the dynamic response of an uncracked DP subjected to the transverse impact loading is computed to determine the locations of the cracks which are liable to start. Establishing a cylindrical coordinate system as shown in Figs. 3, b and 3, c, the dynamic responses of longitudinal stress are presented on the two axial lines: line *1* is $\alpha = 0°$, $r = d/2$, $z > 0$, which is corresponding to the loading area, and line *2* is $\alpha = 180°$, $r = d/2$, $z>0$, which is opposite to the loading zone. For line *1*, the axial stress varying with time and location is sketched in Fig. 12, a, which shows that the maximum axial stress of 595 MPa appears in the middle section of the DP, i.e. section *I-I* in Figs. 3, a and 3, b, at t = 42 ms, when the axial stress contour near this point is presented in Fig. 12, b. Similarly, Fig. 13, a gives the result at the line *2*, in which the maximum axial stress of 394 MPa occurs near the joint (z = 227 mm as shown in Fig. 3, b) at t = 33 ms when the axial stress contour near this point is extracted and shown in Fig. 13, b. At these two locations, crack initiation will most likely occur.

Secondly, circumferential semi-elliptical surface cracks as described in Section 2.1 (a/t = 0.2 and a/c = 0.8) are set at these two extreme positions, denoted as C_1 and C_2 one by one as shown in Fig. 3, b and dynamic responses of the cracked DP are simulated using the developed FE model. In order to avoid the constraints of fixed boundary on the crack, C_1 is set as 100 mm from the fixed end.

Transverse impact from the sidewall excites bending waves and shearing waves in the DP. Due to interaction between the incident wave and reflection wave from boundaries such as fixed ends, the internal and external surfaces of the DP and crack surface, together with the dispersivity of the bending wave, the SIF oscillates violently as time increases. Fig. 14 illustrates the time history of the dynamic SIF K_I^d at the deepest point of crack C_1. It shows that the first peak of 1.4 MPa·m$^{1/2}$ appears at 5.2 ms, and the maximal value of K_I^d of 28 MPa·m$^{1/2}$ happens at 42.2 ms.

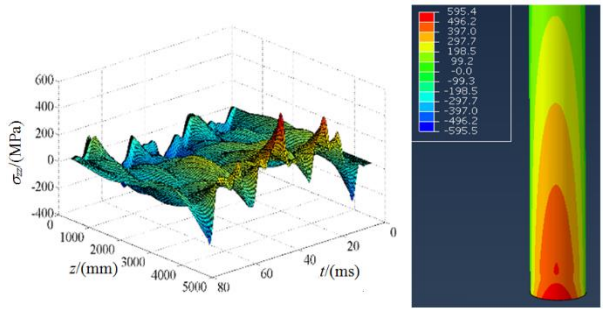

a b

Fig. 12 Axial stress of the uncracked DP: a – on the axial line *1* ($\alpha = 0°$, $r = d/2$, $z > 0$), b – axial stress contour (MPa) near the fixed end at $t = 42$ ms

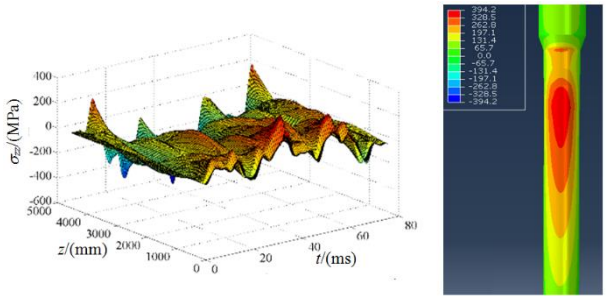

a b

Fig. 13 Axial stress of the uncracked DP: a – on the axial line *2* ($\alpha = 180°$, $r = d/2$, $z > 0$), b – axial stress contour (MPa) near the joint at $t = 33$ ms

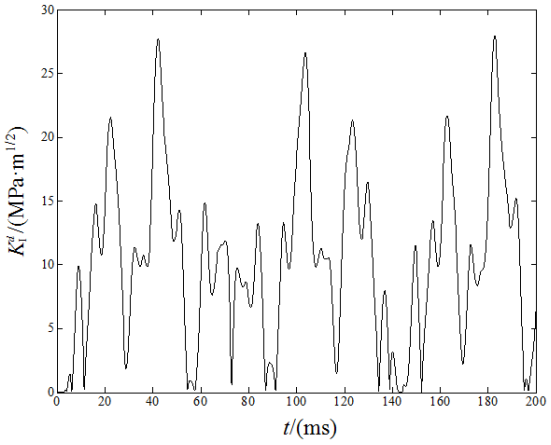

Fig. 14 Time history of $K_{\mathrm{I}}^{\mathrm{d}}$ at point C_1

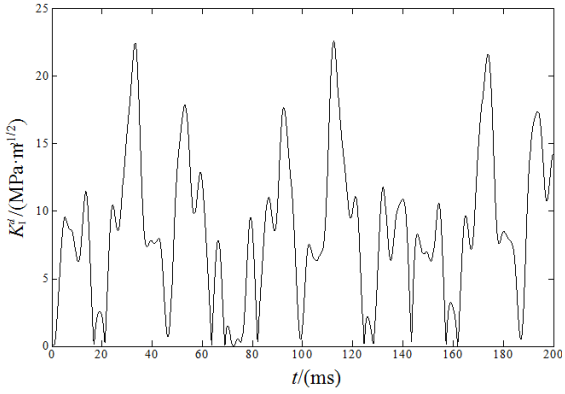

Fig. 15 Time history of K_I^d at point C_2

Fig. 15 presents the time history of K_I^d at the deepest point of crack C_2. The first peak of 9.6 MPa·m$^{1/2}$ appears at $t = 5.4$ ms, and the maximum K_I^d is about 22 MPa·m$^{1/2}$ happening at 33.2 ms. Because the amplitude and number of stress cycles are the key factors for operating life of a DP, collision between DP and borehole wall threatens the safety of the DP seriously.

5. Conclusions

Dynamic behaviours of a defected DP have been simulated under various elementary longitudinal impact loads such as tension, eccentric compression, torsion impact and transverse collision between the DP and borehole wall, which are the components of actual impact loads. A FE model has been developed and the inertial effect of the impact loading on the fracture properties of the cracked DP is evaluated. The main conclusions can be drawn as follows:

1. Under longitudinal impacts, the peak values of dynamic SIFs generally rise with the increase of the loading rate. Dynamic effect due to tensile impact is the most prominent, followed by the torsion impact. Compression shock from down hole has the least influence on the cracked DP. With the crack shape and loading considered in this paper, dynamic SIF is 1.314 times and 1.277 times of corresponding static values under the loading conditions of tension and torsion respectively.

2. As for the transverse collision between the tool joints and the sidewall on the crack driving force of the DP, the middle section of a single DP and the section near the joint are more prone to fracture. Influenced by incident wave from collision exciting, reflection waves from various surfaces and dispersivity of the bending wave, the dynamic SIF oscillates violently, which threatens the safety of the DP seriously.

3. Sharp fluctuation of tensile force or torsion shock, caused by bit bouncing, and violent transverse collision have significant impacts on fracture failure, and the dynamic effects on DP's fracture and fatigue evaluation cannot be ignored.

Acknowledgments

The financial support provided by Open Fund of State Key Laboratory of Oil and Gas Reservoir Geology and Exploitation (Southwest Petroleum University) and Rector's Visiting Fellowships from the UNSW Canberra are gratefully acknowledged.

References

1. **Germay, C.; Denoel, V.; Detournay, E.** 2009. Multiple mode analysis of the self-excited vibrations of rotary drilling systems, Journal of Sound and Vibration 325(1-2): 362-381. http://dx.doi.org/10.1016/j.jsv.2009.03.017.
2. **Moradi, S.; Ranjbar, K.** 2009. Experimental and computational failure analysis of drillstrings, Engineering Failure Analysis 16(3): 923-933. http://dx.doi.org/10.1016/j.engfailanal.2008.08.019.
3. **Zhu, X.H.; Liu, S.H.; Tong, H.** 2010. Comparative study of drill pipe erosion wear in gas drilling and mud drilling, Applied Mechanics and Materials 34-35: 1708-1712.

http://dx.doi.org/10.4028/www.scientific.net/AMM.34-35.1708.
4. **Zhao, G. H.; Li, J.; Zhang, Y. X.; Liang, Z.; Yang, C. H.** 2018. An inverse analysis-based optimal selection of cohesive zone model for metallic materials, International Journal of Applied Mechanics 10(2): 1850015. https://doi.org/10.1142/S1758825118500151.
5. **Raap, C.; Craig, A.D.; Graham, R.** 2011. Drill pipe dynamic measurements provide valuable insight into drill string dysfunctions, SPE 145910. https://doi.org/10.2118/145910-MS.
6. **Lin, X.B.; Smith, R.A.** 1998. Fatigue growth prediction of internal surface cracks in pressure vessels, Journal of Pressure Vessel Technology 120: 17-23. https://doi.org/10.1115/1.2841878.
7. **Carpinteri, A.** 1993. Shape change of surface cracks in round bars under cyclic axial loading, International Journal of Fatigue 15(1): 21-26. https://doi.org/10.1016/0142-1123(93)90072-X.
8. **Predan, J.; Močilnik, V.; Gubeljak, N.** 2013. Stress intensity factors for circumferential semi-elliptical surface cracks in a hollow cylinder subjected to pure torsion, Engineering Fracture Mechanics 105: 152-168. http://dx.doi.org/10.1016/j.engfracmech.2013.03.033.
9. **Itou, S.** 2013. Effect of couple-stresses on the transient dynamic stress intensity factors for a crack in an infinite elastic medium under an impact stress wave, International Journal of Fracture 183: 99-104. http://dx.doi.org/10.1007/s10704-013-9861-0.
10. **Chen, A.J.; Cao, J.J.** 2011. Analysis of dynamic stress intensity factors of three-point bend specimen containing crack, Applied Mathematics and Mechanics (English Edition) 32(2): 203-210. http://dx.doi.org/10.1007/s10483-011-1406-7.
11. **Ariza, M.P.; Dominguez, J.** 2004. Dynamic BE analysis of 3-D cracks in transversely isotropic solids, Computer Methods in Applied Mechanics and Engineering 193: 765-779. http://dx.doi.org/10.1016/j.cma.2003.11.004.
12. **Meng, X.H.; Bai, Z.Y.; Li, M.** 2013. Elastodynamic stress intensity factor for a finite crack in elastic solid under 3D transient loading of Mode I, International Journal of Applied Mechanics 5(4): 1350044. http://dx.doi.org/10.1142/S1758825113500440.
13. **Guo, R.P.; Liu, G.T.; Fan, T.Y.** 2006. Semi-elliptic surface crack in an elastic solid with finite size under impact loading, Acta Mechanica Solida Sinica 19(2): 122-127. https://doi.org/10.1007/s10338-006-0614-8.
14. **Shahani, A.R.; Habibi, S.E.** 2007. Stress intensity factors in a hollow cylinder containing a circumferential semi-elliptical crack subjected to combined loading, International Journal of Fatigue 29: 128-140. https://doi.org/10.1016/j.ijfatigue.2006.01.017.
15. **Zhao, G.H.; Liang, Z.** 2008. Analysis of collision between drillstring and well sidewall, International Journal of Modern Physics B 22(31&32): 5459-5464. https://doi.org/10.1142/S0217979208050656.
16. **Zhang, J.; Zhang, L.; Liang, Z.** 2018. Buckling failure of a buried pipeline subjected to ground explosions, Process Safety & Environmental Protection 114: 36-47. https://doi.org/10.1016/j.psep.2017.11.017.
17. **Enderlein, M.; Ricoeur, A.; Kuna M.** 2003. Comparison of finite element techniques for 2D and 3D crack analysis under impact loading, International Journal of Solids and Structures 40: 3425-3437. https://doi.org/10.1016/S0020-7683(03)00117-3.
18. **Shih, C.F.; Moran, B.; Nakamura, T.** 1986. Energy release rate along a three-dimensional crack front in a thermally stressed body, International Journal of Fracture 30(2): 79-102.
19. **Newman, J.C.; Raju, I.S.** 1984. Stress intensity factor equation for cracks in three-dimensional finite bodies subjected to tension and bending loads, NASA Technical Memorandum 85793, National Aeronautics and Space Administration, Langley Research Centre, Virginia.
20. **Wang, Q.Z.; Zhang, X.; He, Q.Z.; Ren, B.Y.** 1991. A closed form solution for stress intensity factors of shear modes for 3-D finite bodies with cracks by energy release rate method, Acta Mechanica Solida Sinica, English edn 4(1): 75-87.
21. **Chen, Z.G.; Zhang, X.** 1989. A closed form solution of stress intensity factor about a circular tube with a surface crack by energy release bate method, Engineering Fracture Mechanics 32(4): 639-652. https://doi.org/10.1016/0013-7944(89)90196-3.
22. **CAE (Chinese Aeronautical Establishment).** 1993. Handbook of the stress intensity factor, Revised edition. Beijing: Science Press. 809-824p (in Chinese).

G. H. Zhao, L. Zhao, Y. X. Zhang, J. Li

FINITE ELEMENT ANALYSIS OF DYNAMIC FRACTURE BEHAVIOUR OF DRILL PIPE UNDER VARIOUS IMPACT LOADS

S u m m a r y

In this paper, finite element analysis is conducted to study dynamic responses of a defected drill pipe (DP) under impact loading encountered in working conditions. Longitudinal impact loading such as tensile, eccentric compressive and torsional impact loading and transverse collision loading are considered. A finite element model is firstly developed and validated, and then employed to evaluate the effects of various impact loading on dynamic responses of the defected DP. It is found that the inertial effect due to tensile impact is the most prominent among all the longitudinal impact loadings. In addition, the effect of the transverse collision between the DP and the borehole wall on the driving force of the crack is evaluated. It is concluded that the dynamic effects of the various impact loading frequently exerting on the DP should be taken into consideration for life prediction of DPs.

Keywords: drill pipe, three-dimensional crack, dynamic fracture, finite element analysis, impact loading.

Received November 16, 2017
Accepted August 20, 2018